Green Synthesis, Characterization and Photocatalytic Activity of New Photocatalyst $SrCo_2O_4$ Under Visible Light Irradiation

Torkia BOUMETHRED[1], Hadj BENHEBAL[2,*], Ouardia SEBBAH[1], Samir KADI[3], Julien G. MAHY[4], Stéphanie D. LAMBERT[4].

[1]*Synthesis and Catalysis Laboratory, Ibn Khaldoun University Tiaret, Tiaret, Algeria.*
[2]*Department of Chemistry. Faculty of Matter Sciences, Ibn Khaldoun University Tiaret, Tiaret, Algeria.*
[3]*Laboratory of Plant physiology Applied to Above-Soil Culture, Department of Nature and Life Sciences, Ibn Khaldoun University Tiaret, Tiaret, Algeria.*
[4]*Department of Chemical Engineering–Nanomaterials, Catalysis and Electrochemistry, B6a, University of Liege, 4000 Liege, Belgium*

*Author for correspondence; e-mail: benhebalh@yahoo.fr- benhebal@univ-tiaret.dz

Abstract

In order to reduce the enormous costs of photocatalytic processes, the development of new photocatalysts sensitive to visible light constitutes a promising strategy to boost the efficiency of this method in water treatment. In this paper, strontium cobaltite nanoparticles ($SrCo_2O_4$ NPs) was shaped by simple, ecological and economical method using cobalt and strontium nitrates as precursor and freshly isolated chicken egg white as capping agents. The crystalline product $SrCo_2O_4$ NPs was characterized by X-ray diffraction (XRD), Fourier transform infrared spectroscopy (FTIR) and ultraviolet-visible (UV–Vis) spectroscopy studies. The $SrCo_2O_4$-catalyzed Congo red (RC) degradation under visible light is investigated. X-ray diffraction analysis showed that the sample was indeed crystallized in the cubic spinel structure (space group Fd3m). The average size of the nanoparticles was estimated to be ~28 nm. The FT-IR spectrum shows two bands at 620 cm^{-1} and 573 cm^{-1}, which are characteristic of the spinel strontium cobaltite crystalline structure. The two optical band gap energy of synthesised photocatalyst estimated from UV-Visible spectrum are 2.07 and 3,48 eV. The developed photocatalyst exhibits significant photocatalytic degradation of congo red in acidic medium with 97% of the dye mineralized after 5 h.

Keywords: $SrCo_2O_4$; Green synthesis; Egg white; Photocatalysis; Congo red.

Graphical abstract

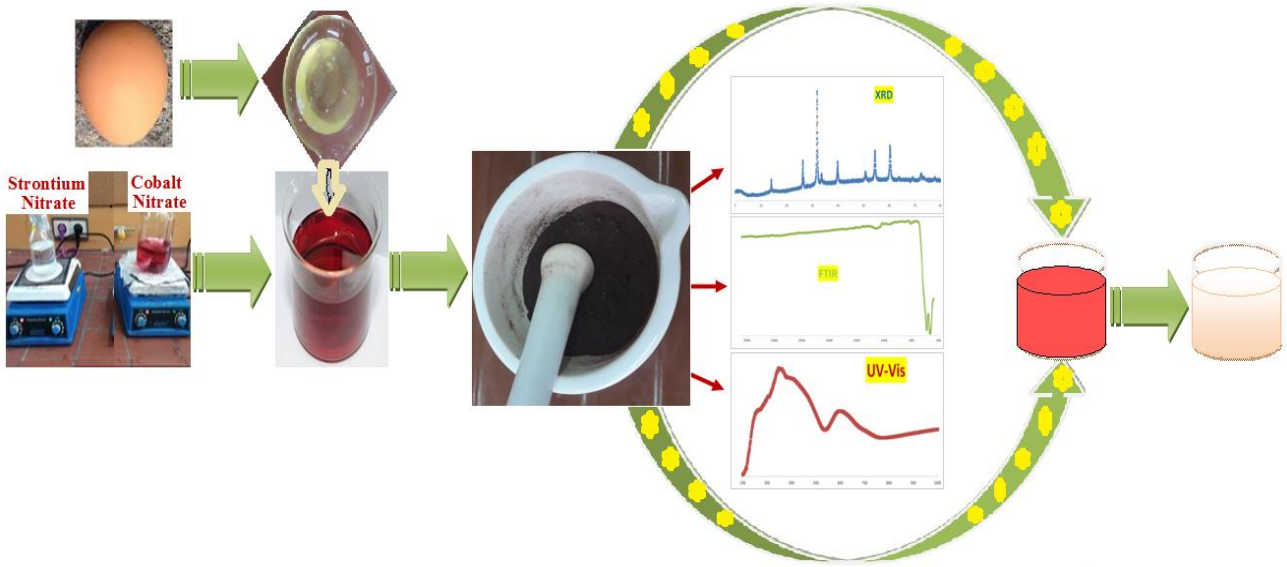

1 Introduction

Since the industrial and agricultural revolution experienced by developing countries, water has become both rare and dangerous due to excessive consumption and pollution[1]. It has been noted that all human activities, particularly in the agricultural and industrial fields, consume a large quantity of water and at the same time generate enormous quantities of wastewater saturated with different species of chemicals and dissolved biological compounds[2,3]. Undoubtedly, the contamination of water resources by effluents loaded with dangerous pollutants such as dyes presents an imminent danger to the environment and in particular to human survival[4]. Due to their multiple industrial uses, organic dyes are produced in very large quantities, the majority of which are diversified without pre-treatment in aquatic environments[5]. With complex structures, dyes are large molecules, chemically stable, which makes their biodegradation difficult[6]. A wide variety of commercially available organic dyes are present in wastewater[7]. Annually, more than 10^5 tonnes of wastewater laden with synthetic dyes discharged directly into the environment[8]. Therefore, it is extremely important to eliminate these polluting substances from wastewater[9]. Among the synthetic colorants widely used in the dyeing process, Congo red dye has been the subject of several research studies due to its high chemical stability, solubility and high toxicity[10]. Faced with increasing water needs, the situation has become extremely worrying, the consequences of which should not be underestimated. Therefore, many biological and physicochemical treatment processes have

been applied to remove dyes from water[11-13]. Among the most dynamic areas of modern science, photocatalysis as a green technology is an ambitious and profitable route, capable of solving many environmental problems through the remediation of wastewater in general and the removal of dyes in particular[14-16]. Over time, given that most photocatalyst materials such as TiO_2, ZnO, WO_3, have a wide bandgap, it has become clear that this technique is only applicable under Ultra Violet radiation. Currently and with the appearance of new opportunities thanks to the developments in the science of nanotechnologies, the application of heterogeneous photocatalysis has been oriented towards the use of new photocatalyst materials sensitive to visible light in order to exploit solar energy and obviate the topic of energy trouble[17]. With a bandgap between approximately 1.45 and 2.7 eV, tricobalt tetroxide (Co_3O_4) with cubic phase is deemed one of the most interesting candidates as photocatalyst in water treatment under visible light[18-21]. The binary metal oxides with general formula MCo_2O_4 (M=Zn, Cu, Mn, Ni, Cd, Fe and Sr) are derived from basic Co_3O_4 spinel p-type semiconductor[22-24]. In addition, a very large number of research studies devoted to the evaluation of the photocatalytic activity of spinel cobalts (MCo_2O_4) have established their photocatalytic superactivity for the degradation of organic dyes[25-29]. A wide variety of physicochemical methods are used today for the synthesis of cobaltite nanoparticles with the chemical formula MCo_2O_4, such as; hydrothermal/ solvothermal methods[30,31], thermal decomposition method[32], sol-gel method[33], Co-precipitation method[29], molten salt method[34], urea combustion method[35] and green chemical method[36-38]. However, the majority of these methods are complicated and expensive because they require complex devices and high energy, which makes their application difficult and consequently, the control of the morphology and particle size distribution, reproducibility and specific surface area of the photocatalyst[39,40]. In addition, the toxicity of precursors constitutes a major problem that chemical synthesis methods must overcome[41]. Compared to all these methods, so-called biological methods are the most beneficial because they are more practical, less expensive, cost-effective and takes less time and effort[42,43]. Additionally, and more importantly, These techniques generates fewer unwanted byproducts and uses non-chemical (biological) compounds as reducing, stabilizing and capping agents[44-46]. In green synthesis, a wide range of biological resources including bacteria[47,48], mushrooms[49,50], yeasts[51,52], algae[53,54], enzymes[55,56], polysaccharides[57], starch[58], egg white[59,60], biodegradable polymers[61], and plant extracts[62-64] are potentially exploited to synthesize inorganic nanomaterials for different fields of application. Indeed, green-synthesized photocatalysts are easily prepared, chemically stable, well crystallized and have excellent photoactivity[65]. Cobalt-based metal oxides

nanoparticles with spinel structure like Co_3O_4, $NiCo_2O_4$, $MgCo_2O_4$, $ZnCo_2O_4$, $CuCo_2O_4$ as well as $FeCo_2O_4$ were greenly synthesized for environmental purposes[24,66-72]. Egg white-mediated green synthesis nanocrystalline materials method is attracting considerable attention. Egg white is a biological liquid consisting essentially of amino acids and proteins[73,74]. Very soluble in water, these amino acids and proteins have a construct that can act as capping agent in nanoparticle production[75,76]. In this paper, green synthesis of strontium cobalt oxide nanoparticles ($SrCo_2O_4$ NPs) attains via eco-friendly method using chicken egg white and observed its photoactivity in the degradation of colored organic dyes in aqueous medium.

2 Experimental Parts

2.1 Materials

The reagents used in this work were of analytical quality and were used without prior treatment: Cobalt nitrate ($Co(NO_3)_2.6H_2O$; Merck. Darmstadt), Strontium nitrate ($Sr(NO_3)_2$, Merck Darnstadt). Stock solution of congo red dye was prepared by adding 10^{-4} mol to 1000 ml of distilled water by continuous magnetic stirring.

2.2 Photocatalyst Synthesis

The spinel oxide strontium cobaltite ($SrCo_2O_4$) nanoparticles were synthesized by green process using the metal nitrates as precursors, egg white as chelating agent. In a typical experiment (Fig.1), appropriate amounts of strontium nitrate [$Sr(NO_3)_2$] and Cobalt nitrate hexahydrate [$Co(NO_3)_2{\cdot}6H_2O$] were separately dissolved in distilled water (Sr:Co molar ratio of 1:2). After complete dissolution, the two solutions were mixed then stirred for 30 minutes. A bright pink solution was obtained (S1). Also, isolated egg white was dissolved in distilled water to give another solution (S2). The solution (S2) is added drop wise to the solution (S1) placed in a water bath at a temperature of 80°C with magnetic stirring. The gel obtained is crushed then calcined at 600°C for 4 hours.

Fig. 1. The preparation steps of $SrCo_2O_4$ nanoparticles.

2.3 Characterization Methods

The X-ray diffraction (XRD) patterns recorded with a Bruker D8 Twin-Twin powder diffractometer using Cu-Kα radiation using a copper anticathode (λ = 1.5406 Å), with a step size of 0.002° and scan speed of 2°/min. FTIR spectra of $SrCo_2O_4$ were studied using a Shimadzu 8400 Spectrometer in the wave number range from 400 cm^{-1} to 4000 cm^{-1}. Ultraviolet-Visible measurements were recorded on a Specord 210 Analytik Jena spectrometer with a holmium oxide filter.

2.4 Photocatalytic Activity test

The photocatalytic activities of $SrCo_2O_4$ were evaluated by degradation of congo red (CR) under visible light irradiation. The suspensions of the dye (10^{-4} M) and the photocatalyst (1 g/L) at different pH (from 2.5 to 6.5) contained in test tubes are placed around the light source (lamp), as shown in Figure 2. The suspensions were stirred for 30 min in dark to reach

equilibrium (photocatalyst-dye molecules) and then, the lamp was lit with continuous stirring and maintaining a constant temperature at 20°C.

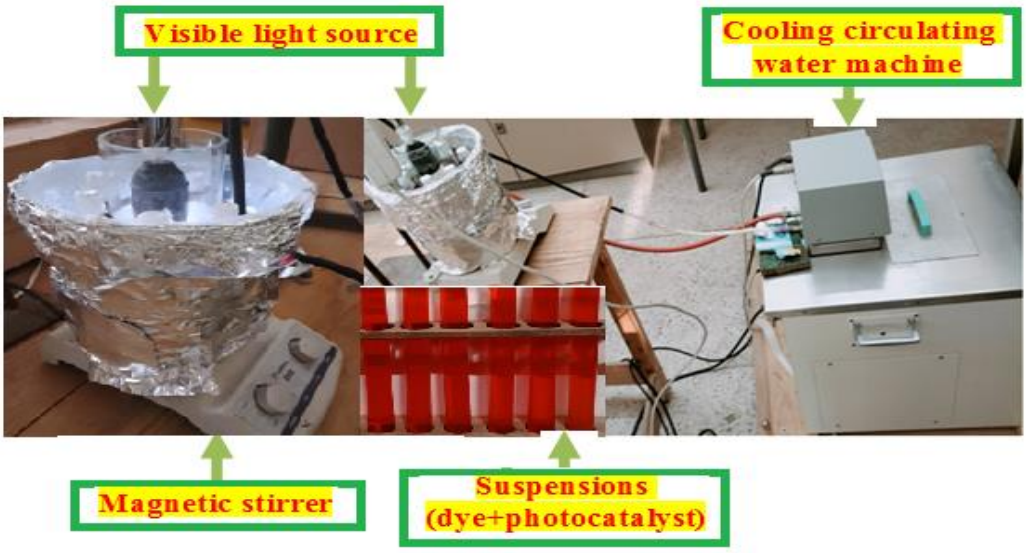

Fig.2. Device used as visible light reactor in the photocatalytic experiments.

3 Results and Discussion

3.1 X-ray Difraction (XRD)

XRD pattern of the $SrCo_2O_4$ powder prepared by green synthesis method and calcined at 600°C for 4 h is shown in figure 3. From figure 3, it is observed that the XRD pattern shows diffraction peaks at the 2 theta values of 19.02, 31.28, 36.83, 38.57, 44.83, 55.73, 59,36 and 65,22°, which are assigned to (111), (220), (311), (222), (400), (422), (511) and (440) crystal planes, which are excellently matching with the standard JCPDS card no. 42–1467, assigned to the face centred cubic phase Co_3O_4[77,78]. To our knowledge, the powder diffraction standards (JCPDS) card assigned to $SrCo_2O_4$ does not exist in the literature. In addition, the high intensity of the reflections and the absence of impurity diffraction peaks indicate the purity and good crystallinity of the prepared $SrCo_2O_4$. The purity of the material was also confirmed by FTIR studies[79].

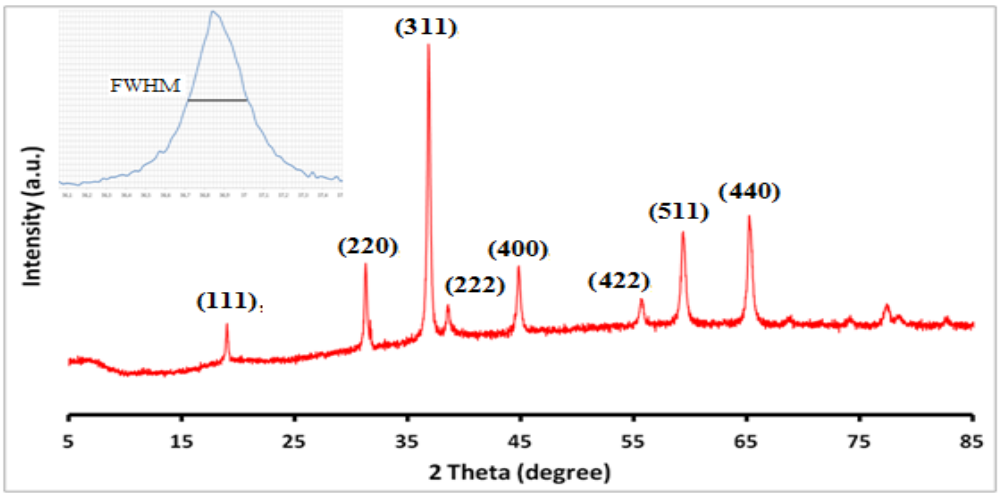

Fig. 3. X-ray diffraction patterns of green synthesized $SrCo_2O_4$

The Scherrer formula was used to estimate the average crystallite size of the nanoparticles from the measured width of their diffraction peaks.

$$\boldsymbol{D = \frac{k\lambda}{\beta cos\theta}} \quad \text{.....(1)}$$

Where k is a constant (=0.9), λ is the used X-ray wavelength, β is the X-ray profile full width at half maximum (FWHM), and θ is the Bragg angle of the considered X-ray reflexion. β and θ were obtained from (220), (311), (400), (511) and (440) orientations.

Based on the equations given below lattice parameter (a), the unit cell volume (V) and the density of the $SrCo_2O_4$ sample can be determined.

$$\boldsymbol{a = d_{hkl}(h^2 + k^2 + l^2)^{1/2}} \quad \text{.....(2)}$$

$$\boldsymbol{V = a^3} \quad \text{.....(3)}$$

$$\boldsymbol{\rho = \frac{8M}{NV}} \quad \text{.....(4)}$$

Where, M = molecular mass of $SrCo_2O_4$ (269.48), and N = Avagadro number (6.023×10^{23}).

The degree of crystallinity (X_C) expressed as the % ratio of the area under the crystalline peaks (X_{Cry}) to the total area (X_{all}) under all peaks (crystalline and non-crystalline), as expressed by equation (3)[80].

$$\boldsymbol{X_C = \frac{X_{Cry}}{X_{All}} x 100} \quad \text{..... (5)}$$

On the other hand, the density of dislocations (δ) linked to the average size of the crystallites by the relation (5), has a significant impact on the crystallographic characteristics of the nanoparticles, because the value of the dislocation density measures the agglomerations of crystal clusters[81,82].

$$\boldsymbol{\delta = \frac{1}{D^2}} \quad \text{(6)}$$

The microstrain (ε) generated in the lattice of synthesised $SrCo_2O_4$ structure is calculated using the following relation:

$$\boldsymbol{\varepsilon = \frac{\beta}{4tan\theta}} \quad \text{(7)}$$

Table 1 summarized the results for crystallite size, lattice parameter, degree of crystallinity, microstrain and dislocation density for the prepared $SrCo_2O_4$ nanoparticles.

Table 1. Average crystallite size (D), cell parameter (a), Unit cell volume (V) degree of crystallinity (X_C), micro-strain (ε) and dislocation density (δ) of $SrCo_2O_4$ nanoparticles.

Average crystallite size (D) (nm)	Cell parameter (a) (Å)	Unit cell volume V $(Å)^3$	Density (g/cm^3)	Degree of crystallinity (X_C)	micro-strain (ε)	Dislocation density (δ)
27,92	**8,086**	**528,69**	**6,77**	**89,37**	**0,00393**	**0,00128**

3.2 Fourier-Transform Infrared Spectroscopy (FTIR)

FTIR analysis was employed to get the information about surface functional groups of molecular precursors and green synthesized $SrCo_2O_4$. The FTIR spectra of the metal nitrates and the strontium cobalt oxide nanoparticles are presented in Figure 4 and Table 2. Practically all vibration modes relating to nitrate are present in the spectra of figure 4(a): the out-of-plane deformation mode (ν_2) at about 829 cm^{-1}. A very weak peak related to the fundamentals of the N-O symmetric stretching (ν_1) is observed at 1053 cm^{-1}. The band at 1380 cm^{-1} is assigned to N-O antisymmetric stretching mode (ν_3). Two combination bands ($\nu_1+\nu_4$) and ($2\nu_4+\nu_1$) are obsreved at 1763 and 2428 cm^{-1}, respectively[83]. From FTIR spectrum of $SrCo_2O_4$ nanoparticles (figure 4(b)), stretching vibrations mode of Co^{3+}-O^{2-} in the tetrahedral sites and Sr^{2+}-O^{2-} in octahedral sites may be observed at 565 and 663 cm^{-1} respectively [84], confirming the formation of pure spinel oxide $SrCo_2O_4$[85,86]. The bands at 1629 and 1630 cm^{-1} are

attributed to water adsorbed on nitrates and $SrCo_2O_4$ surfaces, respectively [87,88]. Water molecules of crystallization present in the nitrate are the cause of the O-H stretching vibrational absorption bands observed at 3400 cm^{-1} [89].

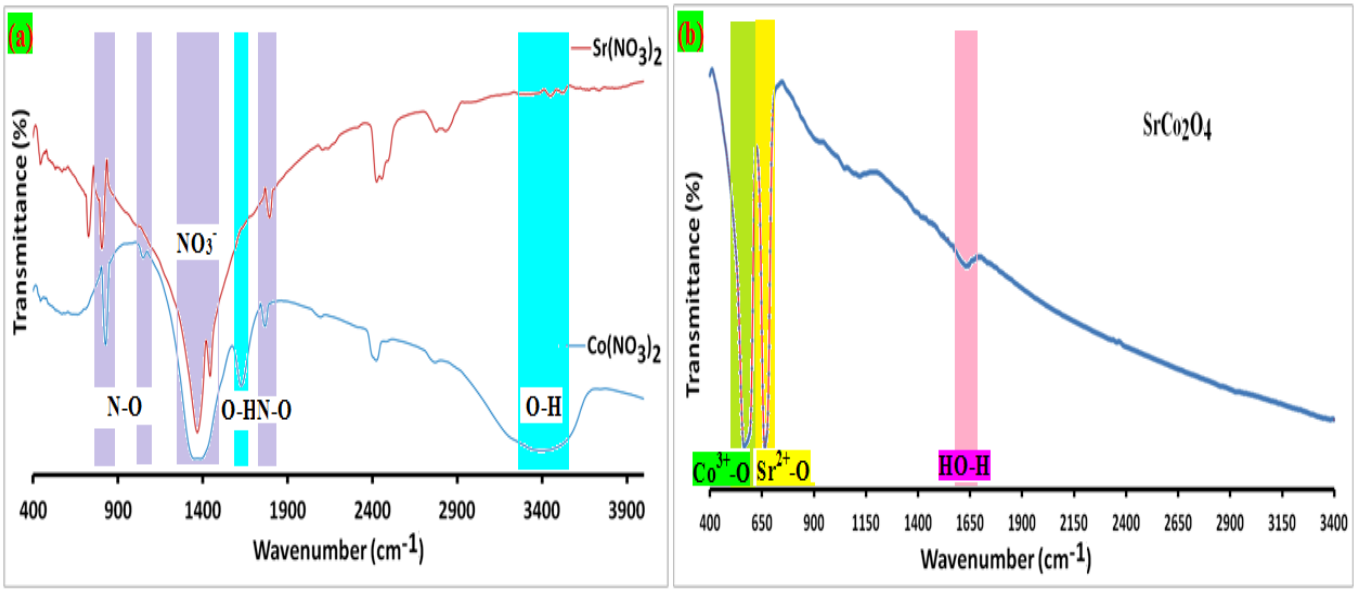

Fig. 4. IR spectra of: (a) Strontium and Cobalt nitrates and (b) Synthesized $SrCo_2O_4$ nanospinel.

Table 2. FT-IR vibrational bands and their assignments of nitrate and strontium cobalt spinel oxide.

Wave number (cm^{-1})		Frequency Assignment	References
Precursors	$SrCo_2O_4$		
	565	Co^{3+}-O^{2-} stretching vibrations mode	84
	663	Sr^{2+}-O^{2-} stretching vibrations mode	84
829		N-O Out-of-plane deformation mode	83
1053		N-O symmetric stretching	83
1380		N-O antisymmetric stretching	83
1629	1630	O-H stretching due to adsorbed water	87
1763		combination band (ν_1-symmetric stretching + ν_4-in-plane deformation) modes	83
2428		combination band ($2\nu_4$-in-plane deformation + ν_1-symmetric stretching) modes	83
3400		O-H stretching due to water of crystallization	89

3.3 Optical Properties

Optical absorption spectroscopy was carried out to determine the optical properties of the synthesized material and accordingly deduce the band gap energies. Absorption UV-Vis

spectrum of as-prepared $SrCo_2O_4$ nanopowders recorded at room temperature is representatively shown in figure 5a. The UV-Vis plot shows two distinct absorption bands at around 356 nm (<400 nm) and 600 (>400 nm). According to literature [85], these bands correspond to the transitions associated with the O^{2-} Sr^{2+} and O^{2-} Co^{3+} charge transfer process, respectively. This spectrum can be converted into Tauc plots (Fig. 5b), who's intercepts of the linear regions extrapolated on the x-axis correspond to the band gap energy of the synthesized sample [90]. The sample displays two direct band gap (Eg_1 and Eg_2) values 2,07 and 3,48 eV, which is the band gap of a crystallized pure spinel cobaltite [91]. O^{2-} to Co^{3+} (Eg_1) charge transfers relating to lower band gap transitions, whereas O^{2-} to Sr^{2+} (Eg_2) charge transfer are assigned to higher band gap changes [92].

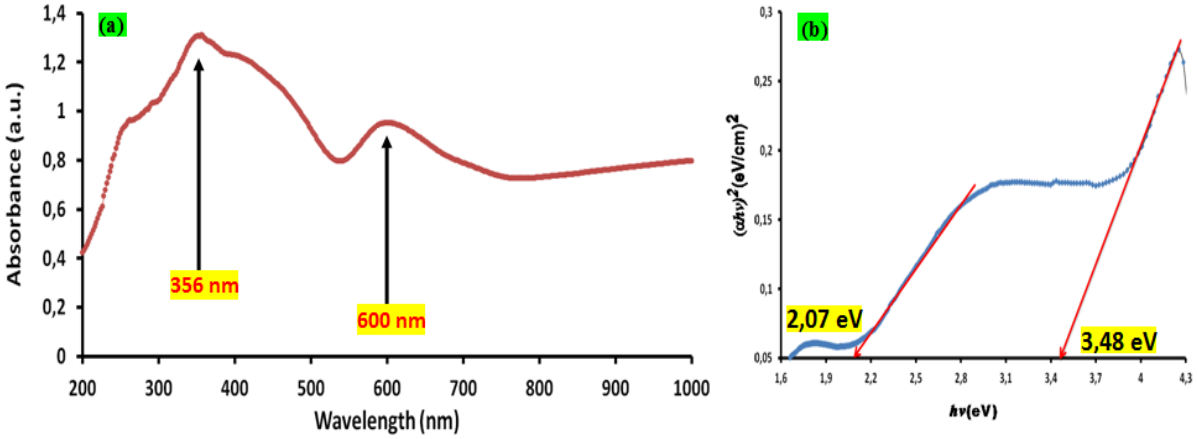

Fig. 5. (a): Reflectance spectra and (b): Band gap based on Kubelka–Munk function of green synthesized $SrCo_2O_4$

3.4 Photocatalytic Activity

The Congo red dye degradation experiments were carried out to evaluate the photocatalytic activity of the as-synthesized $SrCo_2O_4$ NPs. The majority of research studies devoted to the photocatalytic degradation of Congo red have revealed that a higher rate of degradation of CR has been observed in an acidic medium [93-95]. This phenomenon can be justified by the electrostatic attraction linked both to the polarization of the photocatalyst and the anionic nature of the dye [96]. For this reason, our study was carried out by varying the pH of the dye solution in the range from 2.5 to 6.5, while keeping other experimental conditions as constant. Here, pH of the dye solution was balanced using HCl and the initial concentrations of dye and catalyst dosage were set at 10^{-4} mol/l and 1 g/l, respectively. As illustrated in the figure 6, the best photocatalytic performance of the photocatalyst translated by the maximum degradation of the dye was recorded at pH 3. This result has been confirmed

by several studies, and justified by the fact that at this pH value, the electrostatic forces of attraction are at their maximum between photocatalyst's surface positively charged and the negative charge carried by the dye molecules [97-99]. The high photocatalytic activity of the photocatalyst can be attributed to the presence of more active adsorption sites introduced by a high mass/volume ratio due to the low average crystallite size [100]. Compared to other photocatalysts of the Co-based spinels family (Table 3) in the photocatalytic degradation of Congo red dye under visible light, $SrCo_2O_4$ synthesized by green chemistry using egg white as a source of stabilizing agents shows a relatively acceptable photocatlytic activity.

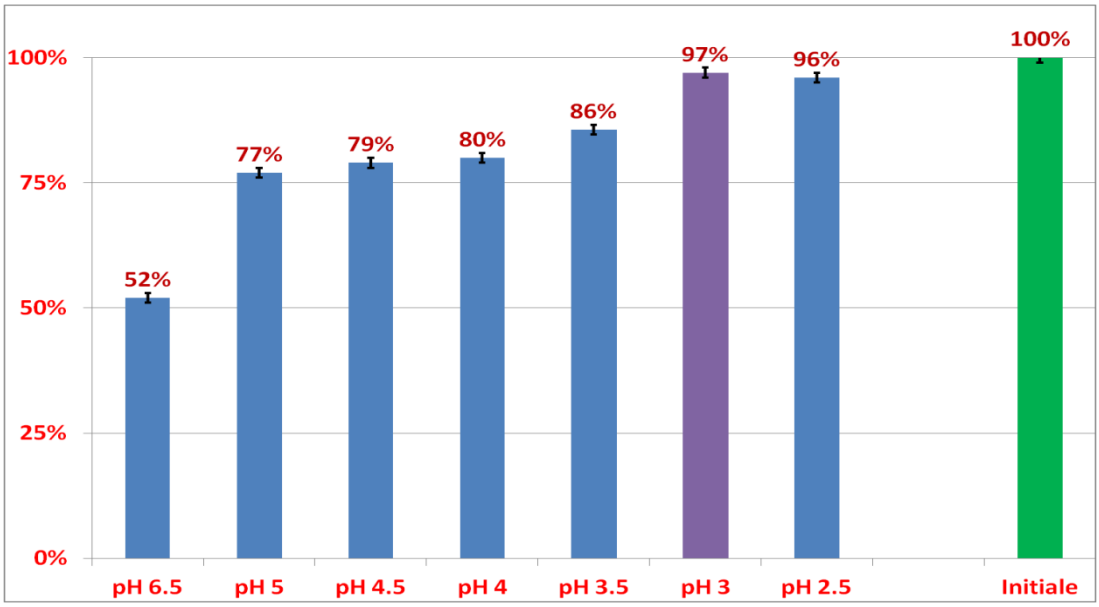

Fig. 6. Photocatalytic degradation rate of CR at different pH

Table 3. Comparing the photocatalytic activity of $SrCo_2O_4$ with different spinel photocatalysts on the degradation of aqueous solutions of congo red under visible light radiation.

Photocatalyst	Catalyst Dose (g L^{-1})	$[CR]_0$ (mg L^{-1})	Degradation Time (min)	Degradation Efficiency (%)	Ref. (year)
$NiFe_2O_4$	0.5	100	60	96.8	101 (2021)
$CoCr_2O_4$	0.2	15	180	94	102 (2023)
$CuCo_2S_4$	0.25	15	80	91.2	103 (2024)
Co_3O_4	0.30	20	240	96	104 (2019)
$CuBi_2O_4$	0.4	30	80	83.39	105 (2024)
$MgAl_2O_4$	1	25	80	99.27	99 (2024)
$ZnFe_2O_4$	1	10	30	95	106 (2018)
Bi Fe_2O_4	1	10	60	77	107 (2018)
$SnFe_2O_4$	0.4	14	120	92	108 (2019)
$ZnCo_2O_4$	-	50	45	98.5	109 (2023)
$CoMn_2O_4$	0.5	5	120	52	110 (2021)
$ZnMn_2O_4$	0.6	20	15	96	111 (2019)
$SrCo_2O_4$	1	70	300	97	[This work]

The probably proposed schematic presentation of the photocatalytic degradation of Congo red on the irradiated surface of $SrCo_2O_4$ is shown in Figure 7.

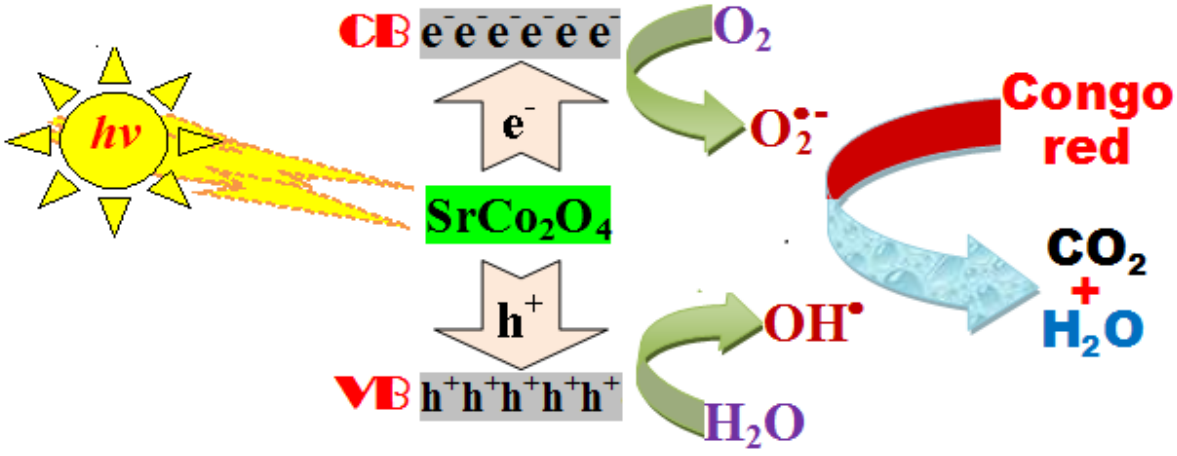

Fig.7. Photocatalytic degradation mechanism of Congo red dye over green synthesised $SrCo_2O_4$ under induced visible light.

The related equations to the mechanism proposed for the photocatalytic degradation of the Congo red dye by green prepared $SrCo_2O_4$ are presented in the following sequence:

$$SrCo_2O_4 + h\nu \rightarrow SrCo_2O_4\,(\boldsymbol{h^+_{VB} + e^-_{CB}}) \quad \text{.....(8)}$$

$$H_2O + h^+_{VB} \rightarrow \mathbf{OH^\bullet} + H^+ \quad \text{..... (9)}$$

$$e^-_{CB} + O_2 \rightarrow \mathbf{O^{\bullet -}_2} \quad \text{..... (10)}$$

$$O^{\bullet -}_2/OH^\bullet + \text{Congo red molecules} \rightarrow \textbf{Mineralized products} \quad \text{.....(11)}$$

4 Conclusion

In summary, with green chemical synthesis route, we obtained $SrCo_2O_4$ nano-sized particles with diameters of around 27,92 nm. The FTIR results are consistent with the XRD data and confirmed the formation of spinel type pure phase $SrCo_2O_4$ nanoparticles. The synthesized photocatalyst show promising optical band gap of 2.07 and 3,48 eV. The photocatalytic performance of the prepared $SrCo_2O_4$ as photocatalyst was evaluated for the degradation of Congo red dye. The high photocatalytic activity of CR dye was observed at low pH value. A rate of 97% photomineralization of the dye was obtained after 5 h.

References

1. M. Farooq and T. Iqbal., *J. Inorg. Organomet. Polym. Mater*. **32**(2022)4422.

2. M. R. Abukhadra *et al*., *J. Inorg. Organomet. Polym. Mater*. **32**(2022)2600.

3. X. Da *et al*., *J. Inorg. Organomet. Polym. Mater.* **32**(2022)2371.

4. T. C. Bessy *et al*., *J. Inorg. Organomet. Polym. Mater*. **33**(2023)3087.

5. P. Srivatsav et al., *Water.* **12**(2020)3561.

6. P. S. Prabhu *et al*., *J. Inorg. Organomet. Polym. Mater.* **32**(2022)999.

7. S.L. Li *et al*., *Cryst. Growth Des*. **10**(2010)1161.

8. S. H. Etaiw *et al*., *J Inorg Organomet Polym.* **27**(2017)1148.

9. X. Wang *et al*., *J. Inorg. Organomet. Polym. Mater.* **28**(2018)800.

10. S. Fındık., *Müh.Bil.ve Ara ş .Dergisi.* **2**(2020)28.

11. A. Zehhaf *et al*., *J. Therm. Anal. Calorim.* **110**(2011)1069.

12. W. Xu *et al*., *New J. Chem.* **40**(2016)2687.

13. L. Chen *et al*., *J. Radioanal. Nucl. Chem*. **292**(2012)1181.

14. M. B. Tahir *et al*., *J. Inorg. Organomet. Polym.* **28**(2018)738.

15. A. Fkiri *et al*., *J. Inorg. Organomet. Polym. Mater.* **33**(2023)2523.

16. I. Ullah *et al*., *J. Inorg. Organomet. Polym. Mater.* **33**(2023)3441.

17. N. Nithya *et al*., *J. Inorg. Organomet. Polym. Mater*. **31**(2021)4594.

18. V. Patil *et al*., *Soft Nanosci. Lett.* **2**(2012)1.

19. S.A. Makhlouf *et al*., *Superlattices. Microstruct*. **64**(2013)107.

20. B. Varghese *et al*., *Adv. Funct. Mater.* **17**(2007)1932

21. A. A. Ismail *et al*., *J. Inorg. Organomet. Polym. Mater.* **33**(2022)1487.

22. J. Mei *et al*., *Prog. Mater. Sci*. **103**(2019)596.

23. J. Samota *et al*., *Poll. Res.* **39**(2020)707.

24. J J. Priya *et al., J. Adv. Sci. Res*. **13**(2022)54.

25. M. Dhanasekar *et al*., *Ceram. Int.* **48**(2022)29460

26. W. Yang *et al*., *Catal. Commun.* **46**(2014)174.

27. S. Hemamalini and R. Manimekalai., *Bull. Mater. Sci.* **44**(2021)154

28. M. Chen *et al*., *Mater. Sci. Semicond. Process.* **146**(2022)106652.

29. R. Rahmatolahzadeh *et al*., *J. Inorg. Organomet. Polym. Mater*. **27**(2017)313

30. L. Duan *et al*., *J. Adv. Ceram*. **2**(2013)266.

31. H. Che *et al*., *Ceram. Int.* **45**(2019)8577.

32. VD. Chinh and NQ. Trung., *J. Nanosci. Nanotechnol.* **15**(2015)4403.

33. M. Guene *et al*., *Bull. Chem. Soc. Ethiop.* **21**(2007)255.

34. M.V. Reddy *et al*., *Cryst. Eng. Commun.* **15**(2013)3568.

35. Y. Liu *et al*., *Chem. Commun*. **50**(2014)14635.

36. Y. Yulizar *et al*., *Materials Letters***. 311**(2022)131465.

37. N. M. Juibari and A. Eslami., *J. Therm. Anal. Calorim*. **130**(2017)1327.

38. R. Yuvasravana *et al*., *Int. j. innov. sci. eng. technol.* **6**(2017)11256.

39. M. Kurian., *J. Aust. Ceram. Soc.* **59**(2023)1161.

40. L. H. Abdel-Rahman *et al*., *J. Inorg. Organomet. Polym Mater.* **32**(2022)1422.

41. X. Tian *et al*., *J. Sol-Gel. Sci. Technol.* **85**(2018)402.

42. S. Ying *et al*., *Environ. Technol. Innov.* **26**(2022)102336.

43. R. Govindasamy *et al*., *Molecules*.. **27**(2022)5646.

44. M. Saeed *et al*., *Waste Biomass Valor* (2023).

45. Z. Zulfiqar et al., *Biocatal Agric Biotechnol.* **57**(2024)103121.

46. M. Amiri and H. Mahmoudi-Moghaddam., *Microchem. J*. **160**(2021)105663.

47. D. Singh et al., *Front. Chem.* **11**(2023)1154128.

48. N. Vosoughian et al., *Microbial. Pathogenesis*. **185**(2023)106457.

49. T. Elsakhawy et al., *Sustainability*, **14**(2022)4328.

50. M. Eskandari-Nojedehi et al., *Green. Process. Synth*. **7**(2018)38.

51. A.M. El-Khawaga et al., *Biomass Conv. Bioref.* (2023).

52. R. Aryadeep., *Indian J. Pharm. Biol. Res*. **8**(2020)26.

53. F. Khan et al., *Chemosphere*. **293**(2022)133571.

54. A E. Alprol et al., *Materials.* **16**(2023)2819.

55. U O. Aigbe and O A. Osibote., *J. Hazard. Mat. Adv.* **13**(2024)100401.

56. I A. Adelere and A. Lateef., *Nanotechnol. Rev.* 5(2016)567.

57. M. Chelu et al., *Int. J. Biol. Macromol.* **211**(2022)410.

58. D. Vaya et al., *Nanoscience & Nanotechnology-Asia*, 8(2018)000.

59. Z. Sabouri et al., *Polyhedron*. **178**(2020)114351.

60. G M. Al-Senani et al., *Crystals*. **13**(2023)1579.

61. K. Handore et al., *J.Macromolecular Sci: Part A: Pure. Appl. Chem.* **51**(2014)941.

62. N. Priya et al., *Front. Nanotechnol.* **3**(2021)655062.

63. S O. Ogunyemi et al., *Artificial. Cells. Nanomedicine. Biotechnology.* **4**(2019) 7341.

64. R D. Kumar et al., *Nanotechnol. Environ. Eng*. **2**(2017)18.

65. S. Sarkar *et al*., Chapter 9. Springer Nature Switzerland AG (2019).

66. F. Al-dolaimy *et al*., J. Inorg. Organomet. Polym. Mater. (2023).

67. L. Velayutham *et al*., *Nanomaterials*, **12**(2022)3668.

68. S. Drummer *et al., Next. Nanotechnology***. 6**(2024)100069.

69. S. Lal *et al., Colloids Surf. A: Physicochem. Eng*. Asp**. 676**(2023)132262.

70. G. Zhang *et al., J. Alloy. Compd.* **942**(2023)169075.

71. N M. Juibari and A. Eslami., *J. Therm. Anal. Calorim.* **130**(2017)1327.

72. J J. Priya *et al., Int. J. Creat. Res. Thoughts*. **10**(2022)d242.

73. K.S. Muthu and P. Perumal., *J. Mater. Sci.: Mater. Electron.* **28**(2017)9612.

74. C. Chang *et al*., *Food. Chem.* **280**(2019)65.

75. H. Kargar *et al*., *Ceram. Int.* **41**(2015)4123.

76. T. Sichumsaeng *et al*., *Int. J. Miner. Metall. Mater*. **29**(2022)128.

77. S. Jayasubramaniyan *et al*., *J. Mater. Sci. Mater. Electron.* **29**(2018)21194.

78. J. Sun, H *et al., J. Porous Materials***. 28**(2021)889.

79. V. Shanmugavalli and K. Vishista., *J. Inorg. Organomet. Polym. Mater*. **30**(2020)1448.

80. E. E. Ateia *et al., J. Inorg. Organomet. Polym. Mater*. **33**(2023)2698.

81. A. M. Abd-Elnaiem *et al., J. Inorg. Organomet. Polym. Mater*. **32**(2022)2209.

82. M. Salah *et al*., *J. Inorg. Organomet. Polym. Mater.* **33**(2023)3195.

83. H B Wu *et al., Aerosol Sci. Technol.* **41**(2007)581.

84. A. Shanmugavani and R.K. Selvan., *Electrochim Acta*, **188**(2016)852.

85. M. Pudukudy and Z. Yaakob., **68**(2014)1087.

86. Y. Z. Wang *et al., Catalysis Letters,* **116**(2007)136.

87. A I. Meky *et al., Scientifc Reports.* **13**(2023)19329.

88. S. Verma *et al., J. Phys. Chem. C.* **112**(2008)15106.

89. M K Trivedi *et al., J Chromatogr Sep Tech.* 6(2015)1.

90. G. Kortüm., *J. Sol-Gel. Sci. Technol.* **61**(2012)1.

91. A.K. Sarfraz and S.K. Hasanain., *Acta Physica Polonica A.* **125**(2014)1.

92. R. S. Reena *et al.*, *Materials Today: Proceedings* **68**(2022)269.

93. S. Darvishi-Farash *et al*. *Environ. Sci. Pollut. Res*. **28**(2021)5938.

94. S. R. Sowmya *et al.*, *IOP Conf. Series: Materials Science and Engineering* **310**(2018)12026.

95. M. Shaban *et al*., *Environ. Sci. Pollut. Res* **27**(2020)22670.

96. T. Tavakoli-Azar et al., *J. Inorg. Organomet. Polym. Mater*. **30**4(2020)858.

97. SB. Narde et al., *Der Pharma Chemica*. **9**(2017)115.

98. E S. Al-Farraj and E A. Abdelrahman., *ACS Omega*. **9**(2024)4870.

99. S M. Sayaya et al., *Int. j. novel Res. phys. chem. Math*. 10(2023)18.

100. I. Maryam *et al*., *Polym. Mater. J. Inorg. Organomet. Polym. Mater*. **33**(2023)3454.

101. P. L. Hariani *et al, Bull. Chem. React. Eng. Catal*. **16**(2021)481.

102. D. Chaibeddra *et al*., *Inorg. Chem. Commun*. **155**(2023)111116.

103. S Nandisha *et al*., *Mater. Sci. Eng. B*. **299**(2024)116992.

104. C. M. Magdalane *et al*., *Surfaces and Interfaces* **17**(2019)100369.

105. E. Haqmal *et al., Colloids Surf. A: Physicochem. Eng. Asp.* **680**(2024)132600.

106. A.Behera *et al*., *Beilstein J. Nanotechnol*. **9**(2018)436.

107. S P. Pattnaik *et al., J. Nanopart. Res.* **20**(2018)1.

108. E. Zhang *et al., J. Sol-Gel. Sci. Technol.* **89**(2019)355.

109. J. Wang *et al., J Mater Sci: Mater Electron.* **34**(2023)531.

110. J A M Mark *et al., Physica B: Phys Condensed. Matter*. **601**(2021)412349.

111. S T. Fardood *et al., Micro & Nano Lett*. **14**(2019)986.